JOURNAL OF SPACECRAFT AND ROCKETS
Vol. 60, No. 6, November–December 2023

Application of Broadband Receptivity Data to the Amplitude Method for Transition Prediction

Simon He* and Xiaolin Zhong†
University of California, Los Angeles, Los Angeles, California 90095

https://doi.org/10.2514/1.A35742

Conventional hypersonic transition prediction relies upon the highly empirical e^N method, which is predicated on theoretical approximations of relative disturbance growth. This does not account for the receptivity mechanism and the high degree of variability present in experimental wind-tunnel conditions, which itself leads to high degrees of variability in transition N factors. The amplitude method, which better approximates the broadband nature of boundary-layer disturbances, was previously proposed to account for the effects of receptivity. In this study, high-fidelity simulated second-mode receptivity data for two blunt cones at Mach 10 to broadband disturbances are applied to an iterative approximation of the amplitude method tuned for second-mode dominated flows. The studied geometries consist of 9.525- and 5.080-mm-nose-radius 7 deg half-angle straight cones based on experimental cases from Arnold Engineering Development Center's wind tunnel 9. Amplitude method predictions show improvement over the accuracy of e^N estimates using standard threshold N factors. In particular, the less blunt 5.080 mm cone demonstrates the best agreement due to its stronger second-mode response. The results of this work provide a preliminary framework for applying high-fidelity receptivity simulations to the amplitude method for transition prediction in hypersonic flows.

Nomenclature

A	=	nondimensional disturbance amplitude
C_{rec}	=	receptivity coefficient
f	=	frequency, Hz
L^*	=	boundary-layer thickness parameter, m
M	=	Mach number
N	=	N factor
T	=	temperature, K
Re	=	Reynolds number
s^*	=	streamwise position, m
α	=	spatial wave number, 1/m
β	=	spanwise wave number
γ	=	freestream noise amplitude
ω	=	circular frequency

Subscripts

e	=	boundary-layer edge
i	=	imaginary component
r	=	real component
T	=	transition location
w	=	wall
0	=	branch I neutral point
∞	=	freestream

I. Introduction

THE primary objective of contemporary hypersonic stability analysis is the development of more efficient and accurate models for transition prediction. The transition to turbulence is known to increase the aerodynamic drag, to significantly affect the control of the vehicle, and to significantly increase heating loads experienced by the vehicle [1–3]. In particular, at these high speeds, thermal loads become the dominant design constraint with turbulent heating rates that can reach upward of three times their laminar counterparts [4,5]. Thus, being able to readily predict the transitionary behavior of a given configuration is critical to designing and optimizing a hypersonic vehicle, particularly in the design of the thermal protection systems necessary for the projectile to survive the extreme conditions encountered during hypersonic flight.

In hypersonic flows, the transition to turbulence is governed by several mechanisms. In the case of weak environmental forcing, through a process called "natural transition," the pathway to turbulence can be broken down into three distinct stages: 1) boundary-layer receptivity to external disturbances, 2) linear growth of small-amplitude disturbances, and 3) nonlinear breakdown of the boundary layer at finite disturbance amplitudes [6]. In the first stage, external disturbance sources such as surface roughness or freestream noise perturb the boundary layer and generate the initial instability waves within the boundary layer through the receptivity mechanism [7,8]. This process involves the conversion of long wavelength external disturbances to the short wavelength boundary-layer modes through a wavelength conversion mechanism. Goldstein described the basic mechanisms of this process, wherein rapidly changing surface geometries at the leading edge and near roughness elements serve to effectively couple these large length-scale external disturbances to the small length-scale boundary-layer modes [9,10]. Although these previous studies were primarily focused on relatively low-speed incompressible flows, the processes have been found to also hold at high speeds and hypersonic flows in particular [11].

However, flow at supersonic and hypersonic conditions results in additional flow features that significantly complicate the receptivity process and the development of boundary-layer instabilities. For one, the presence of a bow shock predicates the direct interaction of external forcing with the boundary layer. Instead, these freestream perturbations first interact with the bow shock to generate complex flow environments behind the shock that then propagate to and force the boundary layer. Due to these shock–disturbance interactions, freestream perturbations composed purely of acoustic, entropy, or vorticity modes can generate shock-layer perturbations consisting of all of the disturbance types behind the shock [12]. Additionally, vehicle designs often incorporate leading-edge bluntness to reduce peak heating loads experienced by the body. In these cases, hypersonic flows about blunted bodies also result in the emergence of significant entropy gradients in the resulting shock layer, which extend outside of the boundary layer until more downstream locations. These entropy layers have been found to reduce local unit Reynolds numbers at the boundary-layer edge, effectively stabilizing

Received 22 March 2023; revision received 11 June 2023; accepted for publication 19 June 2023; published online 24 July 2023.

*Mechanical and Aerospace Engineering Department; simon.he.ucla@gmail.com. Student Member AIAA (Corresponding Author).

†Professor, Mechanical and Aerospace Engineering Department. Associate Fellow AIAA.

the primary second-mode instability in different blunt cone cases [13]. However, recent studies, such as those by Wan et al. [14], have found that isolated low-frequency disturbances excited upstream inside of the entropy layer can be carried to and force primary modal instabilities downstream along the cone after the entropy layer is swallowed.

Due to the importance and complexity of the receptivity process in terms of defining the transitionary pathway for hypersonic boundary layers, it has been studied extensively. In particular, more recent studies have begun to include the effects of more broadband disturbances that better represent the disturbance profiles present in experimental conditions and actual flight. An example of this includes prior work by Balakumar and Kara [15], who attempted to model the broadband receptivity over several sharp and blunt cones using packets composed of multiple discrete frequency waves. Similarly, Goparaju et al. [16] investigated the receptivity of blunted flat plates to stochastic, broadband acoustic forcing to account for potentially unknown tunnel noise conditions. He and Zhong [7,8] instead investigated the receptivity to broadband pulses consisting of freestream acoustic, entropy, and vorticity modes over a selection of blunt cones and identified complex spectral structures in the boundary layer that resulted directly from the broadband freestream forcing. However, although receptivity has been widely studied, there has been relatively little work directly linking the results of receptivity studies to developing transition prediction schemes.

Current transition prediction procedures, such as the e^N method, focus on step 2 of the natural transition pathway and primarily concern themselves with the development of primary modal disturbances. These methods rely on using growth rates for modal instabilities derived from linear stability theory (LST) or the parabolized stability equations (PSEs) to determine the relative amplification of the most unstable boundary-layer disturbance frequencies. Empirically determined amplification threshold values are then used to predict the onset of turbulent transition [15,17,18]. This prediction approach assumes that this relative amplification is the most critical factor in determining transition and often ignores the aforementioned receptivity mechanisms that govern the initial amplitudes of the disturbances themselves. Although this assumption can provide good internal consistency in a given testing environment, transition thresholds based on this methodology can vary significantly between different experiments. For instance, Schneider [19] described experiments with similar nominal freestream conditions that had threshold N factors of five and eight. This difference is attributed to the high degree of variability in freestream noise profiles between different experimental environments. Conventional hypersonic wind-tunnel facilities operate with environmental noise levels far in excess of what is expected in atmospheric flight, and which have not been rigorously quantified. Only recently have more advanced "quiet" wind-tunnel facilities been constructed [20], and more focus been made to characterize the noise profile present in experimental setups [21–23]. In general, the freestream noise in the environment in ground-test facilities is often dominated by acoustic waves radiated from turbulent boundary layers on the tunnel walls [20,21], although freestream turbulence and temperature spottiness can generate vorticity and entropy disturbances as well. Thus, it can be seen that neglecting the receptivity mechanisms that govern the initial shock-layer and boundary-layer disturbance responses can cause significant discrepancies in conventional transition prediction methodologies. Although the standard e^N method is still widely used due to its simplicity, the results of such predictions remain highly empirical and cannot be easily generalized between different test environments without significant corrections.

A number of improved transition prediction methodologies have seen increased interest to overcome some of the limitations of the traditional e^N method. To account for the effects of varying noise levels in the environment, corrected e^N methods have been proposed. Mack [24] initially proposed a variable threshold N factor based on the freestream turbulent intensity of the given experimental environment. This has the advantage of requiring minimal additional computations after the disturbance response and linear growth (N factor) data are first obtained. Crouch and Ng [17] expanded on this methodology to encompass more geometrically complex flows dominated by crossflow instabilities. Although these corrected variable N-factor methods do include the critical effects of receptivity and improve on previous methods with minimal additional complexity, they remain highly empirical and do not sufficiently account for the distributed nature of disturbances in a hypersonic boundary layer. In a more recent development, Paredes et al. [25] also used N-factor correlations combined with a neural network model to predict transition. In their study, they trained a convolutional neural network model using canonical blunt cone cases, which they found to be capable of accurately predicting transition over a wider range of cases.

Recently, there has been some renewed interest on the development of more mechanism-based transition prediction methods that more accurately account for both the receptivity mechanisms and the broadband disturbance profiles present in actual flow. These are based on the amplitude method that was also originally proposed by Mack [24]. The N-factor-based methods discussed previously generally focus on the relative amplification of the single most amplified disturbance frequency. However, this does not adequately represent the highly broadband nature of disturbances that are present in a hypersonic boundary layer [15,24]. Mack's proposed amplitude method suggests integrating across both the spanwise wave number and frequency spectra, centered about the most unstable wave number and frequency, in order to directly estimate the disturbance amplitude level in the boundary layer at a given position. When taken with experimentally measured and correlated breakdown amplitudes, these could then be used to better gauge the beginning of transition in a hypersonic boundary layer. Although similar amplitude method frameworks can potentially be applied to different hypersonic instability mechanisms such as crossflow or Goertler instabilities, current and historical work on the amplitude method has primarily focused on second-mode dominated flows.

Although the general idea behind the amplitude method is straightforward, the broadband dependencies of the governing relation make its efficient application difficult. For instance, although the method requires the disturbance data to be integrated across the frequency and wave number spectra, for a highly amplified discrete mode, only a finite band of disturbances actually contributes in any appreciable amount to the overall amplitude of the perturbation. Correctly identifying and integrating across these variable bands can lead to significant complications in the amplitude method when compared to conventional schemes. As such, recent studies have primarily focused on attempting to simplify the governing amplitude method relation such that it is almost computationally equivalent to the standard e^N methods. Fedorov and Tumin [26] proposed a simplification of the governing integral based on an asymptotic approach to increase the computational efficiency of the method without relying on overly extreme assumptions. Marineau [27], however, expanded upon Mack's original ad hoc approach [24] to suggest a simple iterative approximation for the amplitude method that uses correlations based on both experimental and computational data. Marineau's iterative method [27] in particular remains the most straightforward to apply, with significant experimental and computational results to compare against. As such, this iterative method will be the focus of this study.

In either case, using the amplitude method for transition prediction requires the direct application of receptivity data. However, well-defined environmental noise and high-fidelity receptivity data remain significant limiting factors to the widespread application of the amplitude method [24,26,27]. As such, many prior amplitude method studies used either arbitrarily assumed values or highly empirical correlations for the necessary receptivity response data. Although the receptivity mechanism has been studied extensively, there has been relatively little work directly applying the results of receptivity studies to transition prediction techniques. The primary goal of this work is to link the results of prior high-fidelity receptivity simulations from the broadband studies by He and Zhong [7,8] to Marineau's [27] proposed iterative amplitude method. Contrary to many contemporary broadband receptivity studies, these prior works by He and Zhong [7, 8] produce spectral second-mode receptivity coefficients that directly represent the initial modal instability response to

Table 1 Freestream flow conditions for DNS simulations

Case	R_n, mm	M_∞	$h_{0,\infty}$, MJ/kg	ρ_∞, kg/m^3	ρ_∞, kPa	T_∞, K	U_∞, m/s	Re/m, 1E-6/m
B	9.525	9.79	1.07	0.0427	0.65	51.0	1426	18.95
I	5.080	9.81	1.06	0.0422	0.64	50.8	1425	19.11

broadband freestream forcing of different disturbance types. Simulations in this vein can be used to create general receptivity response databases in a much less resource- and time-intensive manner than conventional experiments. Marineau's iterative method [27] is chosen for its relative simplicity and availability of experimental results for comparison. Additionally, although this iterative amplitude method may be able to be generalized to other disturbances, the correlations in this study are tuned primarily for second-mode dominated flows and do not hold for other disturbance conditions that may be present over a hypersonic body. This study presents a preliminary framework to link future, more robust databases of receptivity data with which the amplitude method can be further generalized for engineering application.

II. Flow Conditions

Marineau's iterative approximation [27] of the amplitude method is applied to two blunt cones at 0 deg angles of attack. These consist of 9.525- and 5.080-mm-nose-radius cones with 7 deg half-angles at Mach 10. The flow conditions for the cases in this study are summarized in Table 1 and correspond to runs 3752 and 3746, respectively, from experiments at the Arnold Engineering Development Center (AEDC) wind tunnel 9 facility [28].

Transitionary behavior on these test cases is determined through application of the amplitude method through the iterative scheme proposed in Ref. [27]. Receptivity data are taken from prior work by He and Zhong [7,8] on these cases, in which the mean flow is converged using a high-order shock fitting method for the laminar direct numerical simulation (DNS). The receptivity of these cases to different broadband freestream disturbances was studied using both linear stability theory and unsteady DNS. The reader is asked to refer to the aforementioned receptivity studies from He and Zhong for additional details on the stability and mean-flow profiles of the investigated cone cases.

III. e^N-Method-Based Transition Prediction

The e^N method is based on amplification factors, called N factors, which are derived from stability theory results. A short overview of the derivation of the linear stability system and the pertinent N-factor relation is given in the following, and the reader may refer to prior work by He and Zhong [7,8] for additional details. First, we begin with the Navier–Stokes system for a compressible, perfect gas flow. The calorically perfect gas assumption is based on the low freestream stagnation enthalpies of the considered cases in Table 1. The system of equations consists of one mass conservation, three momentum conservation, and one energy conservation relation. This can be represented in conservation form as Eq. (1):

$$\frac{\partial U}{\partial t} + \frac{\partial F_j}{\partial x_j} = \frac{\partial G_j}{\partial x_j}, \qquad (j = 1, 2, 3) \tag{1}$$

Although the stability of a system can be studied by solving the full Navier-Stokes system, this can be prohibitively expensive. A simplified version of this system is used in linear stability theory to estimate the growth of the primary disturbance modes in a given flowfield. The LST relations can be derived from the governing Navier–Stokes equations in Eq. (1) by substituting in the instantaneous flow, which can be decomposed into a mean and fluctuating component as in Eq. (2):

$$q(x, y, z, t) = \bar{q}(x, y, z) + q'(x, y, z, t) \tag{2}$$

Here, $q(x, y, z, t)$ is the total instantaneous flow for a given disturbance variable, $\bar{q}(x, y, z)$ represents the mean-flow component, and $q'(x, y, z, t)$ is the fluctuating flow component. This instantaneous flow decomposition is next reintroduced into the governing equations. Because the steady mean-flow component is assumed to satisfy the governing equations, the mean-flow contribution can be subtracted out of the total system. To further simplify the calculations, the mean flow is then assumed to be both axisymmetric/two-dimensional (2-D) and quasi parallel to reduce any remaining mean-flow terms to functions of only y. Using a small disturbance assumption, the system is then linearized to eliminate quadratic and higher-order perturbation q' terms. The system is further simplified by the introduction of a normal mode wave solution in the form of $q' = \hat{q}(y)\exp[i(\alpha x + \beta z - \omega t)]$, where ω is the circular frequency of the disturbance and α and β are the spatial wave numbers of the x streamwise and z spanwise coordinates, respectively. For a spatial stability approach, the circular frequency of a disturbance mode ω, defined as $\omega = 2\pi f$, is manually set at a real number, whereas β is set to zero for a two-dimensional disturbance. This ω is chosen based on whatever particular disturbance frequency is of interest. From these simplifications, the linearized system is further reduced into a set of five ordinary differential equations in the form of Eq. (3):

$$\left(\boldsymbol{A}\frac{d^2}{dy^2} + \boldsymbol{B}\frac{d}{dy} + \boldsymbol{C}\right)\boldsymbol{\phi} = \boldsymbol{0} \tag{3}$$

Here, the vector $\boldsymbol{\phi} = [\hat{u}, \hat{v}, \hat{P}, \hat{T}, \hat{w}]^T$ comprises the disturbance eigenfunctions of the system; and $\boldsymbol{A}$, $\boldsymbol{B}$, and $\boldsymbol{C}$ are complex square matrices of size five. The system can be solved using conventional eigenvalue solution methods, from which the complex spatial wave number of the disturbance can be found. The complex spatial wave number α can be written as $\alpha = \alpha_r + i\alpha_i$, from which $-\alpha_i$ is defined as the growth rate of the disturbance.

Although LST can be used to identify both the growth rates of the disturbances, it does not directly specify their exact amplitudes. Instead, the relative amplification of a given disturbance frequency is represented through the N factor, which is derived by integrating the spatial growth rates in the streamwise direction. This is shown in Eq. (4):

$$e^{N(s,f)} = \frac{A(s,f)}{A_0(f)} = \exp\left[\int_{s_0}^{s} -\alpha_i(s,f)\mathrm{d}s\right] \tag{4}$$

Here, $A(s, f)$ is the local disturbance amplitude, $A_0(f)$ is the initial modal disturbance amplitude, s_0 is the location where the disturbance first becomes unstable at the branch I neutral point, and $-\alpha_i$ is the spatial amplification rate obtained from LST or other stability theory results. Conventional e^N-method-based transition prediction methods simply assume a threshold value for N, which is based on experimental observations. In the case of noisy wind tunnels, it has been found that thresholds of N factors of approximately 5.5 have provided sufficiently accurate transition location estimates [27,29,30].

IV. Amplitude-Method-Based Transition Prediction

As discussed previously, transition predictions have conventionally been done using the e^N method, in which disturbance amplification factors taken from LST or PSE calculations are compared to experimentally correlated threshold values. This process focuses solely on the relative amplification of disturbance waves, and it ignores the absolute amplitudes of disturbances in a hypersonic boundary layer, as well as their highly broadband nature. Due to the varying freestream noise environments and receptivity mechanisms in different flows, this can lead to significant difficulties in relating results between different experiments or flight measurements

with the same nominal mean-flow conditions [19]. These stability-theory-based mechanisms have also seen significant difficulty in addressing the blunt-body paradox [13]. More advanced transition prediction schemes like the amplitude method, as proposed by Mack [24], arose in order to better take into account the effects of receptivity and the multifrequency dependency of instabilities in a hypersonic flow. The governing amplitude method relation used to estimate the local amplitude of an arbitrary disturbance mode is given as Eq. (5):

$$A_d^2(R) = \int_0^\infty \mathrm{d}\left(\frac{\omega\Lambda}{U_1}\right) \int_{-\infty}^\infty A_0^2\left(\frac{\omega\Lambda}{U_1}, \beta\Lambda\right) \times \frac{A}{A_0}\left[\frac{\omega\nu}{U_1^2}, \beta\left(\frac{\nu x}{U_1}\right)^{1/2}; R\right]^2 \mathrm{d}(\beta\Lambda) \tag{5}$$

The relation in Eq. (5) is a generalized expression used to estimate the square of the local disturbance amplitude A_d^2 at a given streamwise position. This streamwise position is denoted in the relation by the local unit Reynolds number $R = (U_1 x/\nu)^{1/2}$. Additionally, Λ represents an external disturbance length scale, ω is the circular frequency of the disturbance, U_1 refers to the freestream velocity, and β is the spanwise wave number of the disturbance of interest. As the amplitude ratio A/A_0 is representative of the relative amplification, or the N factor of a given disturbance mode, this relation can be further recast in dimensionless form as Eq. (6):

$$A_d^2(R) = \int_0^\infty \mathrm{d}\omega \int_{-\infty}^\infty A_0^2(\omega, \beta) e^{2N[\omega,\beta;R]} \mathrm{d}\beta \tag{6}$$

In essence, the relations here estimate the local amplitude of a boundary-layer disturbance mode by integrating both its total frequency and spanwise wave number spectra. Although current applications of the amplitude method have focused on estimating the local amplitudes of the second mode in particular, this general methodology may be applied to a wide variety of boundary-layer disturbance modes as long as the necessary receptivity and amplification data can be acquired. This can include more three-dimensional disturbances like crossflow modes, or even other discrete Mack mode instabilities in the flow. This work will continue to primarily focus on the second-mode disturbance because this mode is generally expected to dominate at most conditions.

Although the generalized amplitude method relation in Eq. (5) and in Eq. (6) is not particularly complex, some difficulties remain that prevent easy widespread engineering application. Among these is a difficulty in identifying relevant frequency and wave number bands because the primary instability modes are highly centered about the most unstable frequencies or wave numbers. Although peak disturbance frequencies can be estimated using boundary-layer edge conditions and general stability profiles, careful selection of pertinent disturbance bandwidths is critical to the amplitude method. This is because the bandwidths can vary significantly between different flows, and overextending the integrated portions of the spectra can dramatically increase the computational cost of the amplitude method. The direct integration of these relations can also be somewhat inefficient when compared to conventional e^N methods, and so contemporary works regarding the amplitude method have presented approximations for these generalized relations to make them more affordable for engineering application. Fedorov and Tumin [26], for instance, suggested an approximation based on an asymptotic approach. This method uses the maximum N factor at a given sampling position, as well as its second-order derivatives in both frequency and spanwise wave number space based on the most optimally amplified frequency and wave number. Although this method is more generalized, it requires significant additional stability computations in the form of N-factor gradients.

Marineau [27] developed an interactive method based on suggested simplifications of the governing relation in Eq. (6) by Mack [24], which are combined with correlated simulation and experimental data. The following analysis will be based on this iterative method because it presents the clearest avenue to directly applying the previously derived receptivity coefficients for case B and case I. The governing relation can be approximated in a form such as Eq. (7) due to the highly concentrated nature of modal instabilities:

$$A_d^2(R) \approx A_0^2(\omega_{\max}, \beta_{\max}) e^{2N_{\max}} \Delta\omega\Delta\beta \tag{7}$$

This approximation is also centered about the most unstable frequency and spanwise wave number of the disturbance, and the broadband scaling is approximated by variable spectral bandwidths of the disturbance in the $\Delta\omega$ and $\Delta\beta$ terms. Although this generalized approximation is widely applicable to many disturbance modes, for the analysis in this study, the primary mode of interest is the second Mack mode. The second mode is two-dimensional in nature, and although it can vary with the azimuthal wave number, this effect is negligible for the preliminary 0 deg angle-of-attack cases considered here. As such, the disturbance amplitude relation can be further simplified by removing the spanwise wave number β dependency. The resulting 2-D amplitude method relation is found in Eq. (8). In this formulation, the integral limits are reduced to a user-defined envelope of frequencies encompassing the most unstable disturbance at a given streamwise position:

$$A^2(s) = \int_{f_1}^{f_2} A_0^2(f) e^{2N(s,f)} \mathrm{d}f \tag{8}$$

Following the simplification suggested by Mack [24] for Eq. (7), the two-dimensional amplitude method relation can be approximated as Eq. (9). Here, C_1 is assumed to be a constant of value 0.48 because Marineau et al. [23] found that this parameter demonstrates minimal variance among the experimental cases corresponding to the simulations considered here. When combined with receptivity as well as linear stability data, this relation can be used to approximate second-mode disturbance levels in the boundary layer:

$$A^2(s) = C_1^2 A_0^2(f) e^{2N(s,f)} \Delta f \tag{9}$$

This relation can be used to establish a variable transition N-factor criterion, which is much more in line with conventional e^N methods in terms of its computational efficiency. Following experimental findings that show that the second-mode amplitudes at breakdown are approximately 60% of the maximum measured disturbance amplitudes [23,27], the final relation is expressed as a transition N factor in Eq. (10). Although the method once more reduces to an N-factor criterion, the breakdown threshold is not defined through the N factor in this case. Instead, the total growth of the initial disturbance modes from the receptivity response is compared to correlated breakdown amplitudes. The resulting N factor is simply compared to the stability profile of the given flow to determine a transition location:

$$N_T = \ln\left(\frac{1.25 A_{\max}}{A_0(f_T)}\right) \tag{10}$$

Beginning with an initial estimate of the expected transition location, correlations are used to predict both the maximum disturbance amplitude near breakdown as well as the initial amplitude of second-mode disturbances in the boundary layer. These values are applied to the final transition N-factor relation in Eq. (10), which when combined with the LST-derived maximum N-factor envelope can be used to iteratively prediction the transition location of the given flow. The necessary correlations and results of this implementation are discussed and compared with Marineau's results [27] in the following sections.

V. Receptivity Coefficients

To directly use the amplitude method to predict transition, receptivity data are critical to determine the initial disturbance levels in the boundary layer. By using a generalized database of receptivity coefficients along with measured or computationally derived tunnel noise conditions, the initial broadband disturbance levels in a given

hypersonic boundary layer can be estimated. Although the derivation of these generalized receptivity relations and noise profiles is critical to the development of amplitude method-based tools, the current state of available data remains somewhat limited. In this study, prior broadband receptivity data from He and Zhong [7,8] are used, which consist of the boundary-layer responses to freestream broadband fast acoustic, slow acoustic, entropy (temperature), and vorticity disturbances. The derivation and results of this receptivity analysis are discussed in a condensed form here for completeness, but the reader is asked to refer to the aforementioned papers for additional details.

The response of the system to each freestream disturbance environment can be represented through a receptivity coefficient. The receptivity coefficient in this study $C_{\text{rec}}(f)$ is defined as the initial amplitude of the second-mode disturbance at the branch I neutral point for a given discrete frequency f normalized by the freestream disturbance content of the same frequency. This coefficient is determined using a combination of LST and unsteady DNS through a decomposition recommended by Schneider [20] and Huang [31]. The purpose of this decomposition is to attempt to isolate the contribution of the primary second-mode disturbance from the highly broadband boundary-layer profile excited by the freestream pulse disturbances. By selectively sampling the unsteady DNS data at a streamwise location expected to be dominated by the primary mode of interest, the local N factor as derived from stability theory can be used to calculate the approximate initial amplitude of the disturbance at the branch I neutral point. Assuming significant second-mode amplification, the receptivity coefficients for the second mode can be derived in this manner through Eq. (11):

$$C_{\text{rec}}(f_n) = A_0(f_n) = \frac{A(s^*, f_n)}{e^{N(s^*, f_n)}} \tag{11}$$

Here, $A(s^*, f_n)$ is the Fourier decomposed surface pressure amplitude and $e^{N(s^*, f_n)}$ is the exponentiated N factor determined through LST for a given frequency f_n and a streamwise sampling point s^*. Because the most dominant instability mode for the investigated cases is expected to be the two-dimensional second mode and the cases of interest are held at a 0 deg angle of attack, spanwise variation in both the unsteady DNS and LST results was ignored.

When this process is repeated for each frequency in the destabilized second-mode band, the full second-mode receptivity spectra can be derived. An example of the receptivity coefficient spectra used in this work is shown in Fig. 1. Data for the 9.525-mm-nose-radius case (case B) are taken from Ref. [7], and data for the 5.080-mm-nose-radius case (case I) are taken from Ref. [8]. The receptivity coefficients for case I were compared against simulations for a similar 5.08 mm cone case from Balakumar and Chou [15], which demonstrated good agreement with available data for the slow acoustic disturbances.

Slightly different definitions of the receptivity coefficient are also quite prevalent in the literature. Similar to the works of Balakumar and Chou [15] and Kara et al. [32], a standard receptivity coefficient is defined as the boundary-layer disturbance normalized by the freestream noise level at the computed branch I neutral location. This essentially ignores the decomposition method presented earlier in this paper and incorporates the full broadband disturbance profile present in the boundary layer, including any potential nonmodal components. Because the receptivity coefficients for the planar pulses in these cases were found to vary significantly between the decomposed and un-decomposed methods [7,33,34], the un-decomposed receptivity coefficients are also used. These are plotted for both cones in Fig. 2.

A. Correlations for Marineau Iterative Amplitude Method

Marineau's iterative process [27] requires the use of several correlations to approximate the freestream noise profile present in the flowfield, the initial amplitude of the second-mode disturbance in the boundary layer, the maximum boundary-layer disturbance amplitudes near breakdown, and the resulting N factors near breakdown. These correlations are derived from a combination of LST data, DNS data, and experimental measurements. First, the second-mode breakdown amplitudes will be considered. Citing prior work by Fedorov and Kozlov [35] and Casper et al. [36], it was found that the maximum breakdown amplitude of the second-mode disturbances can be correlated with the edge Mach number of the flow. Although these prior studies suggested a linear variation between maximum second-mode breakdown amplitudes, the AEDC wind tunnel 9 results over a selection of sharp and blunt cones are best fit using a power law variation. This correlation is shown in Fig. 3, which demonstrates good agreement between the fit and the experimental data.

To correctly apply this breakdown amplitude correlation, the edge Mach number conditions must be accurately defined. The boundary-layer thickness δ_e has traditionally been described using a velocity criterion that stipulates that the boundary-layer edge is located where the local velocity reaches 99% that of the freestream. Although this is applicable in general to low-speed flows, it is not necessarily valid for hypersonic conditions. Instead, a stagnation enthalpy criterion is used due to the fact that the stagnation enthalpy is expected to remain constant in the inviscid flow outside of the boundary layer [37]. The boundary-layer edge is assumed to be the point at which the stagnation enthalpy of flow reaches 99.5% of the freestream value. The resulting profiles for case B and case I are compared against calculated results for corresponding cases from Paredes et al. [38] and Marineau [27] in Fig. 4. The resulting edge Mach number profiles are observed to

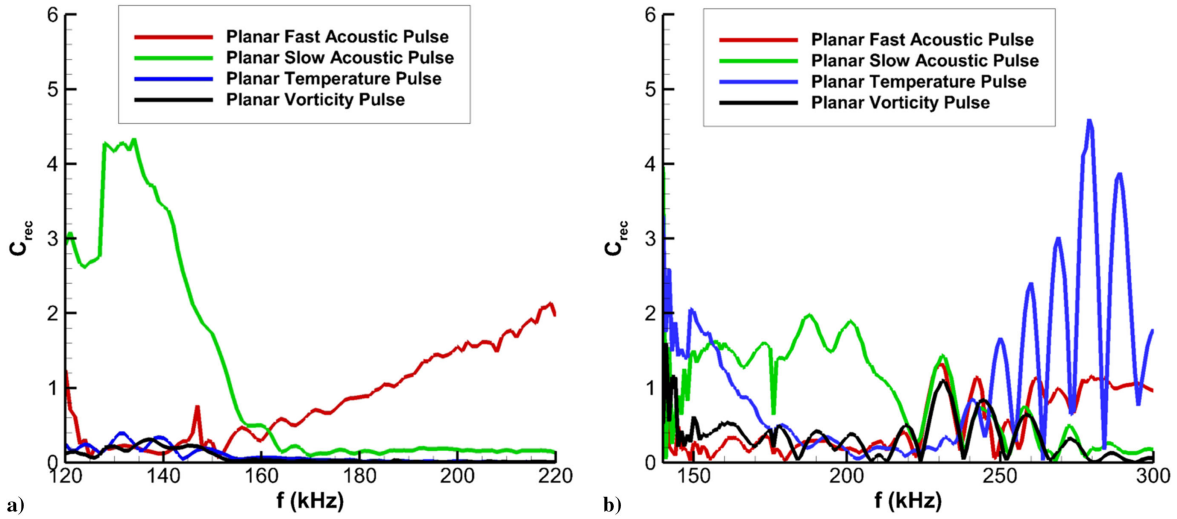

Fig. 1 Decomposed receptivity coefficient spectra for planar pulse disturbances in a) case B and b) case I. Results for case B are reproduced with permission from He and Zhong [7] (copyright by the authors). Data for case I reproduced with permission from He and Zhong [8] (copyright by the authors).

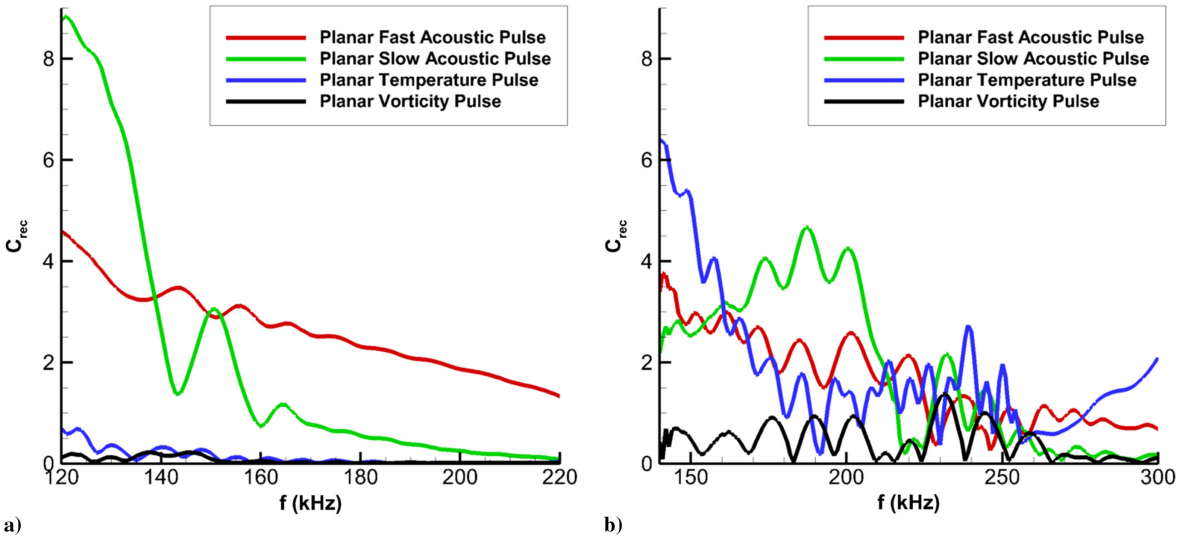

Fig. 2 Un-decomposed receptivity coefficient spectra for planar pulse disturbances in a) case B and b) case I.

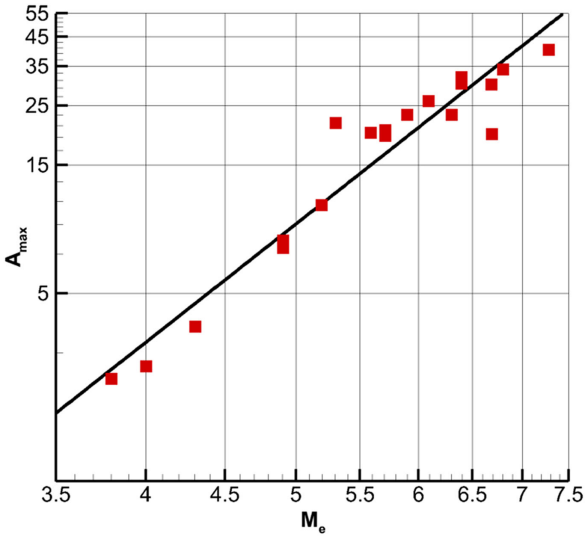

Fig. 3 Correlation of edge Mach number vs maximum breakdown amplitude based on experimental data. Reproduced from works of Marineau et al. [27,28].

demonstrate excellent agreement with both Paredes et al.'s [38] and Marineau's [27] presented profiles, and as such will be applied to the generalized second-mode breakdown amplitude correlation.

Now, a method to approximate the initial amplitudes of the second-mode disturbances is required. This is done by applying receptivity correlations to estimates or measurements of the freestream noise spectrum present in the flowfield. Following the simplifications suggested by Mack [24], the reduced amplitude method integral in Eq. (7) is seen to be centered about the most amplified frequency with an assumed bandwidth parameter of $\Delta f = f_{\max}/4$. Again, because these cases are primarily concerned with two-dimensional disturbances, the contribution of the spanwise wave number β is disregarded. This maximum second-mode frequency can be determined using either an LST- or PSE-derived stability profile for the given mean flow, along with initial guess of the transition location. The resulting maximum disturbance frequency profiles derived from LST results for both case B and case I are depicted in Fig. 5.

After this maximum LST frequency is taken from the LST data, it is used to find the amplitude of the incident freestream disturbance at the same frequency. Marineau et al. [23] provided the approximate freestream noise profile as a corrected fit of pitot pressure measurements from other AEDC wind tunnel 9 experiments under similar conditions. This is given in Fig. 6.

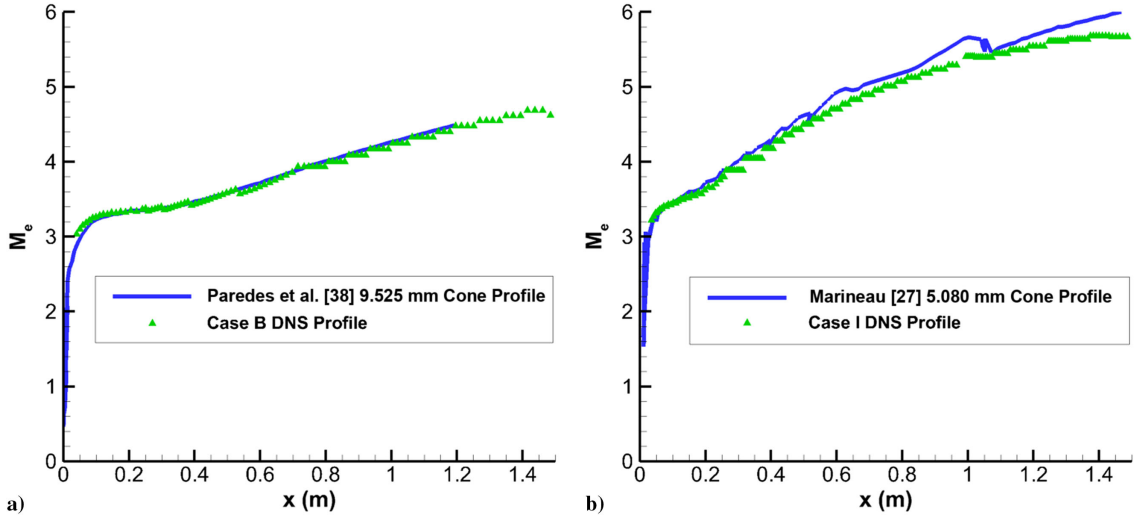

Fig. 4 Edge Mach number profile using 99% total enthalpy criterion for a) case B compared to work of Paredes et al. [38] and b) case I compared to work of Marineau [27].

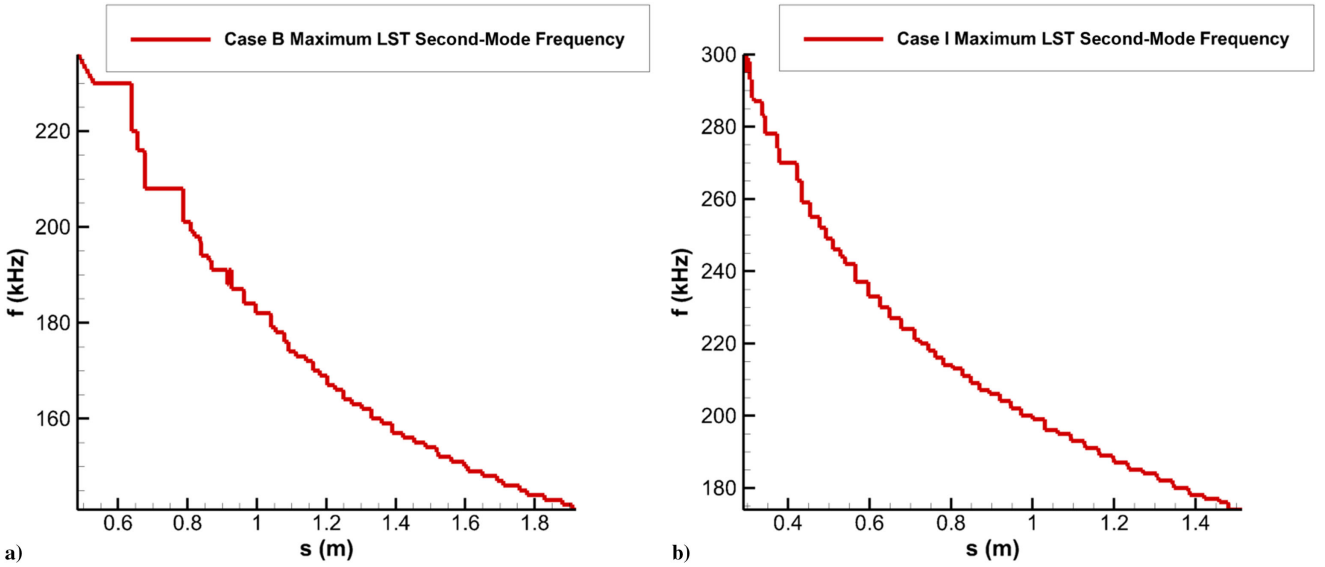

Fig. 5 Maximum LST second-mode frequency vs streamwise location for a) case B and b) case I.

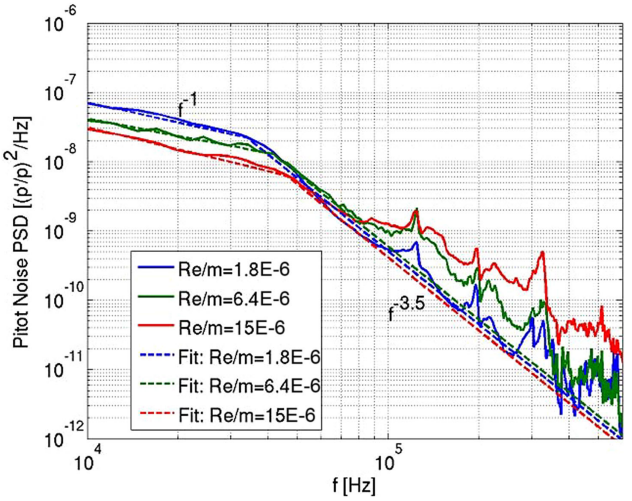

Fig. 6 Normalized pitot pressure noise measurements for freestream disturbances, reproduced from work of Marineau et al. [23].

The low-frequency disturbances for each case demonstrate excellent agreement with an f^{-1} frequency fit. Following this, the spectral noise roughly matches an $f^{-3.5}$ fit at frequencies higher than approximately 40 kHz. The higher-Reynolds-number cases demonstrate distortions in this slope, as well as strong noise at higher frequencies. Marineau et al. [23] attributed these to increased noise sensitivity due to the higher Mach numbers of these cases, as well as acoustic wave reflection between the probe and the local shock. Assuming that such distortions do not necessarily reflect the actual freestream spectra, we elect to continue using the linear fit as suggested by Marineau [27] and Balakumar and Chou [15]. The freestream noise amplitude, referred to as γ_0, at the maximum disturbance frequency is given in Eq. (12):

$$\gamma_0 = \sqrt{\frac{C}{2}\Delta f (f_{\max})^{-3.5}} \tag{12}$$

The γ_0 term is the incident amplitude of the freestream disturbance, $C = 126.5E6$ is a linear fit parameter from Ref. [15] based on data reported in Ref. [23], and $f_{\max}$ is the maximum second-mode frequency at the given streamwise location taken from the LST profile. The receptivity magnitude coefficients are simply defined as the disturbance amplitude response at a given frequency normalized by the freestream disturbance level. To convert between these data and the freestream noise amplitude correlations as provided by Marineau et al., the receptivity coefficients are further renormalized with respect to the boundary-layer edge pressure. Therefore, following the same procedures as Marineau [27], the total initial amplitude at the local maximum disturbance frequency is simply defined as $A_0(f\,\max) = C_{\text{rec}}(f_{\max})\gamma_0$.

Finally, the total maximum N-factor envelope is necessary in order to iterate on and refine the initial estimate of the transition location. The resulting LST-derived N-factor envelopes are shown in Fig. 7 for both the case B and case I mean flows. Due to the reduced nose bluntness, the second-mode response is expected to be significantly stronger for case I. This is reflected well in the N-factor plots because the overall N factors for case I are shown to be significantly larger than that of case B throughout the cone domains. At the end of the cones, case I has a peak N factor of approximately 14.6, whereas case B peaks at an N factor of 9.3. This further reinforces contemporary and historical findings that nose bluntness delays the development of the primary second-mode instability [13,28,39].

B. Iterative Amplitude Method Results

Following the methodology and correlations discussed previously, the transition locations of case I and case B can be estimated using receptivity field data for each of the four canonical disturbance types in the freestream. These consist of freestream fast acoustic, slow acoustic, temperature (entropy), and vorticity disturbances. The finite pulse results from Refs. [7,8] are not used because the isolated nose forcing is not expected to as accurately replicate the extensive noise profile present in a wind-tunnel test environment. First, an initial estimate is made of the transition location. Using this initial guess, the local maximum second-mode frequency as well as the edge Mach number are calculated from LST and DNS profiles. From these values, the local second-mode breakdown amplitude as well as the freestream noise amplitude are estimated using the correlations presented in the previous section. Receptivity coefficient data are combined with the freestream noise correlations to generate initial second-mode amplitudes, which are used in concert with the breakdown amplitude estimates to calculate the local transition N factor. Using the N-factor envelope taken from LST, this value is used to identify an updated guess for the transition location, which is iterated upon through the same process until convergence.

The predicted transition locations using the iterative method described previously are plotted for case B in Fig. 8. Additionally, due to the strong variations in the receptivity spectra found between the decomposed and un-decomposed data, results using both approaches are presented. The un-decomposed spectral receptivity coefficients are derived by directly sampling the unsteady DNS at the

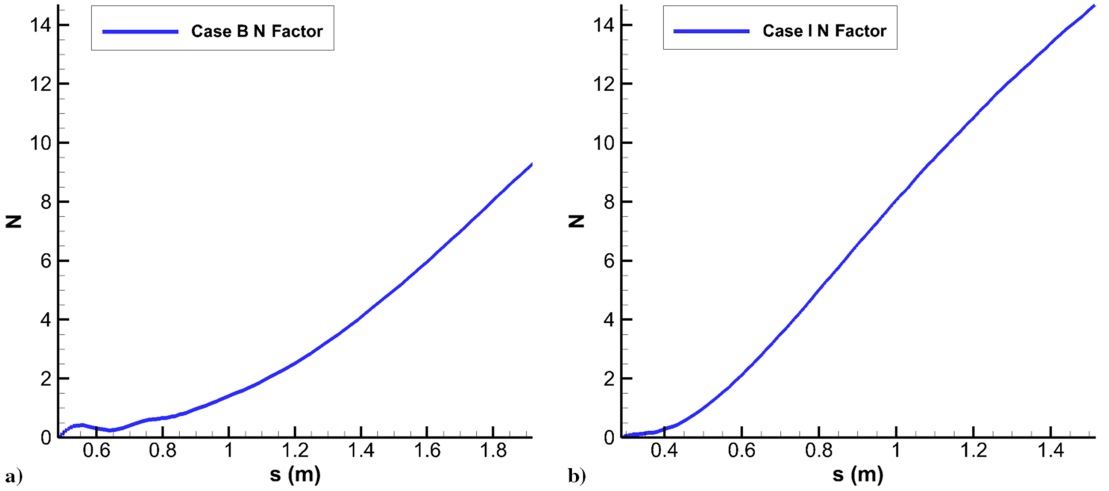

Fig. 7 Maximum LST *N* factor vs streamwise location for a) case B and b) case I.

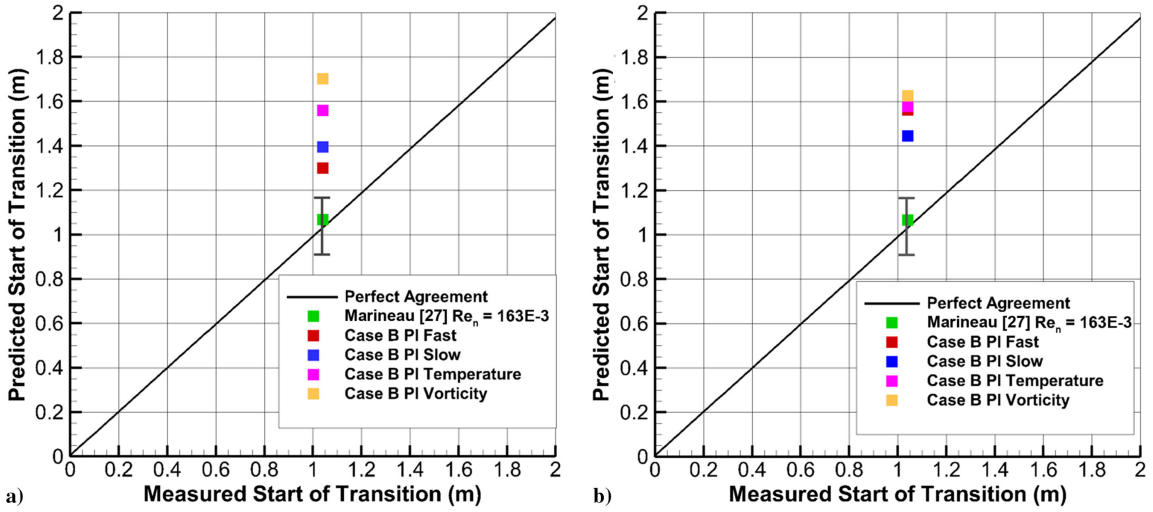

Fig. 8 Predicted transition locations vs measured results for case B (9.525 mm) after planar pulse forcing using a) un-decomposed and b) decomposed second-mode receptivity coefficients.

LST-calculated branch I neutral stability points. Additional details on the differences between the decomposed and un-decomposed receptivity coefficients applied here can be found in Refs. [7,34]. An error bar for the uncertainty in the experimentally measured transition location is also shown in the figure. This error is derived from the limited distribution of pressure transducers in the original experiment [28]. The case B results demonstrate significant divergence from Marineau's [27] reported experimental and numerical transition results, and for the most part lie outside of the reported uncertainty region. On average, this ranges from 60 to 30% error for the un-decomposed results, whereas the decomposed results range from approximately 60 to 40% error when compared to the experimentally measured transition location of 1.04 m. In both cases, the acoustic pulse data converge most readily toward the experimental result, with the fast acoustic pulse complying with the best in the un-decomposed receptivity coefficient cases and the slow acoustic results complying with the best for the decomposed receptivity coefficient cases.

Similar transition location results are plotted for case I in Fig. 9. Once again, Marineau's results [27] along with the same experimental error are shown in the figure. The uncertainty in the transition location is fixed due to similar limitations in sensor placement. It can be observed that the agreement for the case I transition location is significantly better than it was in case B, with more of the planar pulse results remaining within the estimated uncertainty range. Looking at the un-decomposed receptivity case in Fig. 9a, every data point other than the vorticity pulse lies within the experimental uncertainty range. The errors here range from approximately 21% for the vorticity pulse to 12% for the fast acoustic pulse. The decomposed receptivity coefficient results in Fig. 9b diverge more from the measured transition position, with only the slow acoustic pulse result falling within the uncertainty range. Here, the error ranges from approximately 39% for the temperature pulse to 17% for the planar slow acoustic pulse. These errors are relative to the experimental transition location of 0.68 m. Similar to case B, the acoustic pulses demonstrate the best agreement. This is likely attributed to the greater receptivity response observed at the primary second-mode frequencies for the acoustic pulses in both case B and case I.

The results of this iterative amplitude method can be compared against predictions made using the conventional e^N method. To make this comparison, a standard noisy wind-tunnel transition N factor of 5.5 is used [27,29,30]. Using the LST-predicted N-factor curves in Fig. 7, the predicted transition locations for the e^N method are at streamwise positions of 1.55 m for case B and 0.83 m for case I. These e^N method predictions have errors of approximately 40% for case B and 22% for case I. In both cases, this is comparable to the temperature and vorticity pulse results using the un-decomposed receptivity coefficients, whereas the acoustic receptivity data resulted in improved accuracy. This indicates that the amplitude method, even in this highly preliminary form, is capable of improving on common established practices.

Figure 10 similarly shows the transition point N factor predicted by the iterative method vs the N factor at the measured transition

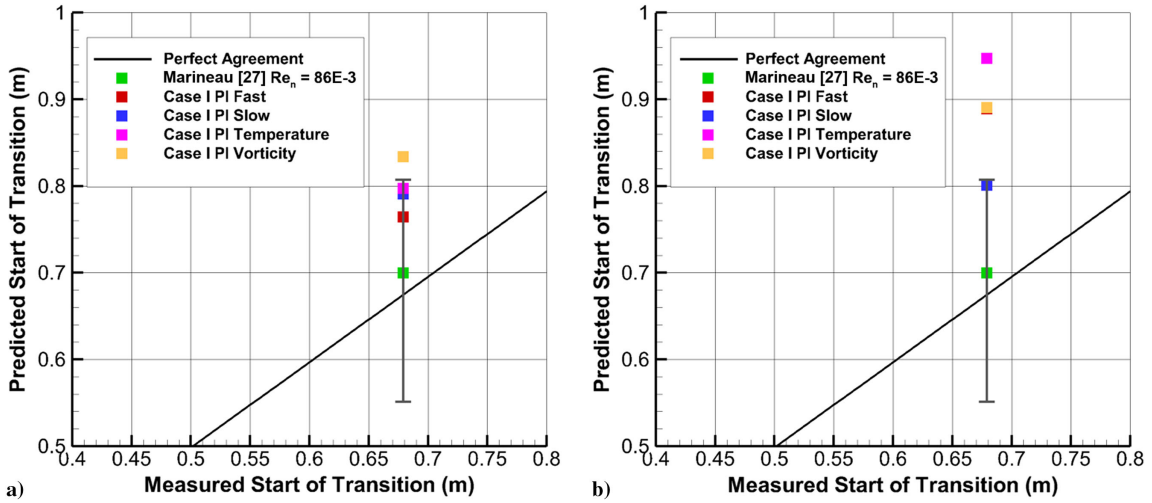

Fig. 9 Predicted transition locations vs measured results for case I (5.080 mm) after planar pulse forcing using a) un-decomposed and b) decomposed second-mode receptivity coefficients.

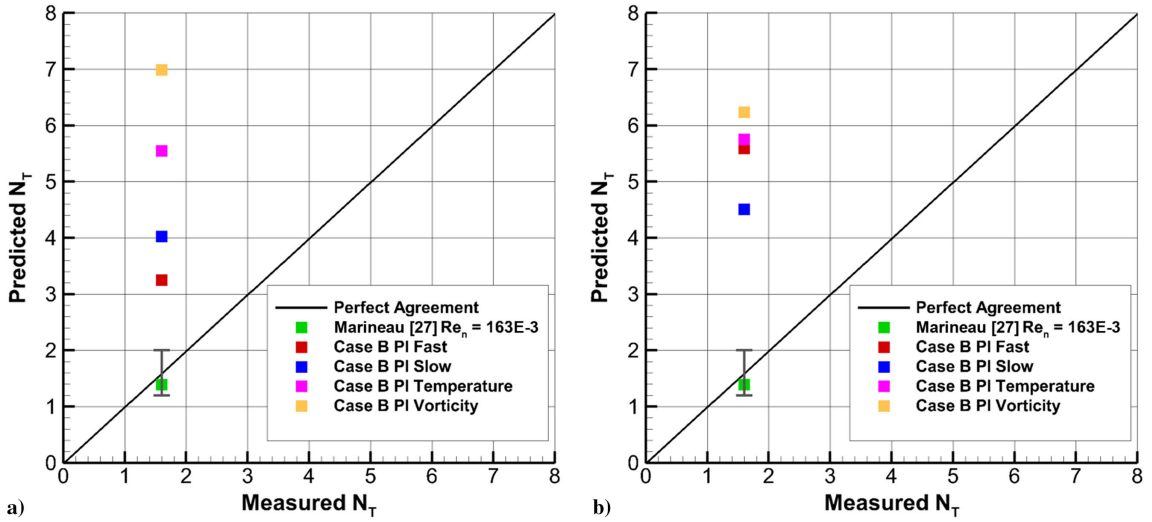

Fig. 10 Predicted transition *N* factors vs measured results for case B (9.525 mm) after planar pulse perturbation using a) un-decomposed and b) decomposed second-mode receptivity coefficients.

location for case B using both decomposed and un-decomposed receptivity data. The uncertainty here is taken from Marineau et al. [28], and it is once again based on the uncertainty in the measured transition location due to pressure sensor placement. Once more, significant disagreement is observed for every disturbance type, although the acoustic disturbances are closest to the measured results for both the decomposed and un-decomposed receptivity data. Qualitatively, the accuracy of the transition *N* factor is much worse than the transition location results. This is directly related to the disagreement in the prior transition location results because the previously observed overprediction of the transition location directly causes overprediction in the transition *N* factor due to the monotonicity of the *N*-factor profile for case B in Fig. 7a. This may be partially explained by the relatively weak second-mode amplification observed in case B and its respective experimental counterpart in the work of Marineau et al. [28].

Similar transition *N* factors for case I are presented in Fig. 11. Again, case I adheres more closely to the experimental result due to the stronger second-mode response. However, the overprediction of the transition location for case I in Fig. 9 also uniformly results in overprediction for the transition *N* factor because the *N*-factor curves in Fig. 7 increase monotonically against the streamwise position for both cones. The un-decomposed results in particular are closest to both the experimental transition location and transition *N* factor in both case B and case I. This is due to the overall larger receptivity coefficient from the un-decomposed spectra, which results in larger initial disturbance amplitudes that are more in line with what Marineau [27] observed. This requires less modal amplification to reach the necessary breakdown amplitudes.

The general disparity between the computed results here and Marineau's measured result [27] can be attributed directly to differences in the initial input receptivity coefficients. In particular, the receptivity coefficients taken from Refs. [7,8] seem to underpredict the receptivity coefficients of the optimal disturbance Marineau [27] used. For Marineau's run 3752, which corresponds to case B, Marineau reported a peak receptivity coefficient of approximately 3.7. For run 3746, which corresponds to case I, he saw a slightly lower peak receptivity coefficient of 2.85. These were calculated by solving Eq. (10) for $A_0(f_T)$ using the measured maximum breakdown amplitude $A_{\max}$ and an *N* factor calculated through stability theory. The peak case B planar pulse receptivity coefficients were found to be approximately 1.2 for the most amplified frequency in the un-decomposed spectra, which correspond to the planar fast acoustic result. At the same conditions for case I, the peak coefficient was found to be approximately 1.9, which again corresponded to the fast acoustic disturbance in the un-decomposed spectra. The lower receptivity coefficients from this study signify reduced boundary-layer disturbance responses, and subsequently lower-amplitude

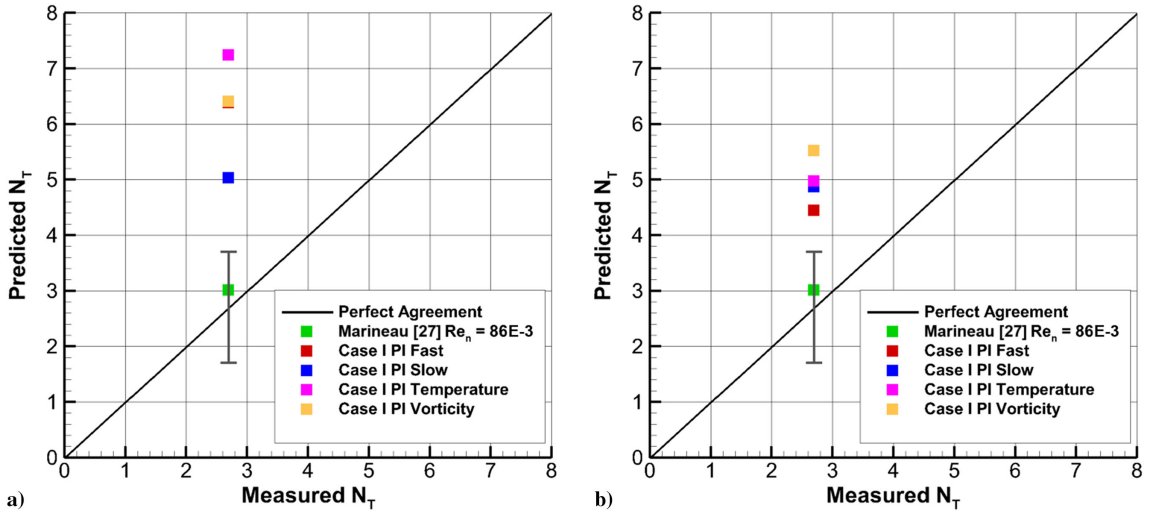

Fig. 11 Predicted transition *N* factors vs measured results for case I (5.080 mm) after planar pulse perturbation using a) un-decomposed and b) decomposed second-mode receptivity coefficients.

initial disturbances in the boundary layer. These require additional amplification before they reach the experimental breakdown amplitudes and trigger transition. This, in turn, pushes the expected transition location further downstream and increases the expected *N* factor at transition, which explains the large overprediction of both the transition location and transition *N* factor demonstrated in the results here. The overall larger receptivity coefficients of the un-decomposed spectra, which are due to the included influence of more disturbances outside of the second mode, explain the better general agreement between the computed transition location using the un-decomposed receptivity data vs the decomposed receptivity data. Additionally, there are some differences between the computational cases here and Marineau's own study, which may also contribute to the divergence of results. Namely, different approaches to calculating freestream viscosity led to unit Reynolds numbers in case B and case I, being up to 15% higher than their experimental counterparts [7,8]. This leads to stronger second-mode growth, which itself results in an upward shift of transition *N* factors.

VI. Discussion

In this work receptivity data for a selection of broadband, freestream pulse disturbances are applied to an iterative approach to the amplitude method. Although there has been a long history of research in both the receptivity mechanism as well as in developing improved transition prediction methods, there has been relatively little work attempting to link the two. In particular, although the amplitude method requires receptivity data to directly estimate boundary-layer disturbance amplitudes, the source of these data is often based on assumed values or highly empirical correlations. This study presents a preliminary attempt to apply high-fidelity receptivity data taken from simulation to an approximation of the amplitude method that is more directly applicable to contemporary experimental cases. Although some deficiencies have been identified, the results have laid a framework for the further improvement of the amplitude method through the integration of analytical receptivity data taken from DNS. The receptivity data used here were taken from prior work by He and Zhong [7,8] for broadband pulse disturbances consisting of canonical fast acoustic, slow acoustic, entropy, and vorticity disturbances in the freestream. The approximate amplitude method is based on simplifications originally suggested by Mack [24] and Marineau [27] for flows dominated by the two-dimensional second mode. The correlations for threshold breakdown amplitudes and freestream noise levels are based on experiments performed at the AEDC wind tunnel 9 facility [28].

Prior observations demonstrated significant differences in the receptivity spectra based on whether or not a decomposition method was used to attempt to isolate the primary second-mode disturbances [7,33]. As such, both decomposed and un-decomposed receptivity data were applied to the iterative scheme used in this work. In both case B and case I, the un-decomposed receptivity data resulted in significantly better agreement with both the computed transition locations for Marineau [27] and the measured transition locations from Marineau et al. [28]. In particular, the resulting errors for the acoustic pulse cases were significantly improved against conventional e^N predictions using threshold *N* factors of 5.5 [27,29,30]. The un-decomposed receptivity data resulted in better predictions primarily due to the higher overall receptivity coefficients found in that case. However, in general, the results using the broadband spectral receptivity coefficients from He and Zhong [7,8] demonstrate notable divergence from the experimentally measured transition location when compared to Marineau's [27] own computed results.

This disagreement can be traced to differences in the receptivity coefficients used to solve for the initial second-mode amplitudes. In particular, although the broadband pulse receptivity coefficients from He and Zhong [8] were found to compare well against slow acoustic results from Balakumar and Chou [15], they were much lower than the receptivity coefficients reported by Marineau [27]. The question now remains, "What is the source of this large disparity in the receptivity coefficients?" For one, Marineau used a decomposition based on linear stability that was applied to experimentally measured breakdown amplitudes. At these points, there could have been significant nonlinear disturbance interactions that were not captured in the receptivity studies by He and Zhong [7, 8]. Additionally, uncertainties exist with the general freestream profile that are critical to correctly determining the receptivity response of the flow. The freestream noise profile, presented as normalized pitot tube measurements in Fig. 6, was not directly measured for the investigated cases and was instead based upon measurements for prior experiments with similar freestream Reynolds numbers [23,40]. This leads to some uncertainty in the actual freestream noise conditions of the given cases. Furthermore, it is well known that the types of incident disturbances can have dramatic differences on the overall receptivity behavior, both in terms of the peak magnitudes of the boundary-layer disturbances as well as the disturbance bands that are excited [6,8,41]. Although the data provided here give a distribution of environmental pressure disturbance amplitudes, they do not depict the composition of disturbances present in the experimental environment. Previous work has shown that acoustic radiation from turbulent wall boundary layers is expected to dominate in similar tunnel environments fields [21,22], although more thorough characterization of the environmental noise through both experimental measurements and simulations is critical to the correct application of receptivity coefficient data on a case-by-case basis.

The phase coherence of the incident pulse disturbances may also play a significant role in terms of the receptivity data. Recent work by Egorov et al. [42] has shown that the receptivity response over flat

plates can be highly dependent on the coherence of the forcing. In particular, they showed that incoherent forcing with a randomized disturbance phase can result in much stronger disturbance growth than similar conditions for coherent disturbances. He [34] found that broadband pulse disturbances with a coherent phase, such as those used for the receptivity data applied here, can generate significant modal interference in the boundary layer. In some cases, this interference can result in significant reductions in second-mode disturbance amplitudes, whereas other modal instabilities are instead amplified. This may partially explain the reduced receptivity coefficient found for case B and case I in He and Zhong's work [7, 8] when compared to the experimentally derived result from Marineau's work [27]. However, these findings are fairly novel and have not been confirmed over a wide range of conditions. As such, they require additional study to confirm, especially in the more complex flow environment present over a blunt cone.

VII. Conclusions

This study documents an initial attempt to link high-fidelity receptivity simulations to a more direct engineering-oriented application of Mack's amplitude method [24]. Using this method, the transitionary behavior of a given hypersonic vehicle can, ideally, be predicted in an accurate and efficient manner in cases where the second mode dominates. It should be noted that the framework shown here is not necessarily applicable to other sources of hypersonic transition such as crossflow, Goertler, or attachment line stabilities without additional consideration. Receptivity modeling remains a significant bottleneck to the continued development of the amplitude method. Improvement has been shown using the simple broadband receptivity coefficients here with regard to baseline estimates from the conventional e^N method. Nonetheless, there remains significant room for improvement in this implementation of the amplitude method. For instance, due to the preliminary nature of this work, the used broadband receptivity coefficients remain focused on two-dimensional disturbances and do not represent the flow response profiles for cases with more oblique profiles, such as flight at angles of attack. Additionally, uncertainties remain with regard to factors such as disturbance phase coherence and the freestream noise profiles present in different experimental environments that require additional study before further generalizations can be made. Although these challenges must be addressed to continue developing the amplitude method for engineering application, this preliminary study's results indicate the potential for integrating high-fidelity analytical receptivity data taken from simulation into transition prediction.

Acknowledgments

This research was partially supported by the U.S. Air Force Office of Scientific Research (AFOSR) under AFOSR grant no. FA9550-19-1-0206, monitored by Ivett Leyva and Sarah Popkin; and by Office of Naval Research grant no. N00014-17-1-2343, monitored by Eric Marineau. Primary computational resources were provided by the Extreme Science and Engineering Discovery Environment (XSEDE) and the Advanced Cyberinfrastructure Coordination Ecosystem: Services and Support (ACCESS) programs through the Texas Advanced Computing Center and the San Diego Supercomputer Center under grant number TG-ASC090076, which is supported in part by the National Science Foundation. Additional computational support was provided by the U.S. Department of Defense High Performance Computing Modernization Program through project AFOSR40 702004. The views and conclusions contained herein are those of the authors and should not be interpreted as necessarily representing the official policies or endorsements, either expressed or implied, of the U.S. Air Force Office of Scientific Research, the Office of Naval Research, XSEDE, ACCESS, or the U.S. Government.

References

[1] Fedorov, A., "Transition and Stability of High-Speed Boundary Layers," *Annual Review of Fluid Mechanics*, Vol. 43, No. 1, 2011, pp. 79–95. https://doi.org/10.1146/annurev-fluid-122109-160750

[2] Reshotko, E., "Hypersonic Stability and Transition," *Hypersonic Flows for Reentry Problems*, Vol. 1, No. A93-42576 17-02, Springer, Berlin, 1991, pp. 18–34, https://ntrs.nasa.gov/citations/19930058582.

[3] Zhong, X., and Wang, X., "Direct Numerical Simulation on the Receptivity, Instability, and Transition of Hypersonic Boundary Layers," *Annual Review of Fluid Mechanics*, Vol. 44, No. 1, 2012, pp. 527–561. https://doi.org/10.1146/annurev-fluid-120710-101208

[4] Schneider, S. P., "Hypersonic Laminar-Turbulent Transition on Circular Cones and Scramjet Forebodies," *Progress in Aerospace Sciences*, Vol. 40, Nos. 1–2, 2004, pp. 1–50. https://doi.org/10.1016/j.paerosci.2003.11.001

[5] Knisely, C., Haley, C. L., and Zhong, X., "Impact of Conical Hypersonic Boundary Layer Transition on Skin Drag and Heating," *AIAA SciTech 2019 Forum*, AIAA Paper 2019-1134, 2019. https://doi.org/10.2514/6.2019-1134

[6] Ma, Y., and Zhong, X., "Receptivity of a Supersonic Boundary Layer over a Flat Plate. Part 3. Effects of Different Types of Free-Stream Disturbances," *Journal of Fluid Mechanics*, Vol. 532, June 2005, pp. 63–109. https://doi.org/10.1017/S0022112005003836

[7] He, S., and Zhong, X., "Hypersonic Boundary-Layer Receptivity over a Blunt Cone to Freestream Pulse Disturbances," *AIAA Journal*, Vol. 59, No. 9, 2021, pp. 3546–3565. https://doi.org/10.2514/1.J059697

[8] He, S., and Zhong, X., "The Effects of Nose Bluntness on Broadband Disturbance Receptivity in Hypersonic Flow," *Physics of Fluids*, Vol. 34, No. 5, 2022, Paper 054104. https://doi.org/10.1063/5.0088236

[9] Goldstein, M., "The Evolution of Tollmien-Schlichting Waves near a Leading Edge," *Journal of Fluid Mechanics*, Vol. 127, Feb. 1983, pp. 59–81. https://doi.org/10.1017/S002211208300261X

[10] Goldstein, M., "Scattering of Acoustic Waves into Tollmien-Schlichting Waves by Small Streamwise Variations in Surface Geometry," *Journal of Fluid Mechanics*, Vol. 154, May 1985, pp. 509–529. https://doi.org/10.1017/S0022112085001641

[11] Balakumar, P., and Kegerise, M. A., "Receptivity of Hypersonic Boundary Layers over Straight and Flared Cones," *AIAA Journal*, Vol. 53, No. 8, 2015, pp. 2097–2109. https://doi.org/10.2514/1.J053432

[12] McKenzie, J. F., and Westphal, K. O., "Interaction of Linear Waves with Oblique Shock Waves," *Physics of Fluids*, Vol. 11, No. 11, 1968, pp. 2350–2362. https://doi.org/10.1063/1.1691825

[13] Lei, J., and Zhong, X., "Linear Stability Analysis of Nose Bluntness Effects on Hypersonic Boundary Layer Transition," *Journal of Spacecraft and Rockets*, Vol. 49, No. 1, 2012, pp. 24–37. https://doi.org/10.2514/1.52616

[14] Wan, B., Su, C., and Chen, J., "Receptivity of a Hypersonic Blunt Cone: Role of Disturbances in Entropy Layer," *AIAA Journal*, Vol. 58, No. 9, 2020, pp. 4047–4054. https://doi.org/10.2514/1.J058816

[15] Balakumar, P., and Chou, A., "Transition Prediction in Hypersonic Boundary Layers Using Receptivity and Freestream Spectra," *AIAA Journal*, Vol. 56, No. 1, 2018, pp. 193–208. https://doi.org/10.2514/1.J056040

[16] Goparaju, H., Unnikrishnan, S., and Gaitonde, D. V., "Effects of Nose Bluntness on Hypersonic Boundary Layer Receptivity and Stability," *AIAA SciTech 2020 Forum*, AIAA Paper 2020-1818, 2020. https://doi.org/10.2514/6.2020-1818

[17] Crouch, J., and Ng, L., "Variable N-Factor Method for Transition Prediction in Three-Dimensional Boundary Layers," *AIAA Journal*, Vol. 38, No. 2, 2000, pp. 211–216. https://doi.org/10.2514/2.973

[18] Reed, H. L., Saric, W. S., and Arnal, D., "Linear Stability Theory Applied to Boundary Layers," *Annual Review of Fluid Mechanics*, Vol. 28, No. 1, 1996, pp. 389–428. https://doi.org/10.1146/annurev.fl.28.010196.002133

[19] Schneider, S., "Effects of High-Speed Tunnel Noise on Laminar-Turbulent Transition," *Journal of Spacecraft and Rockets*, Vol. 38, No. 3, 2001, pp. 323–333. https://doi.org/10.2514/2.3705

[20] Schneider, S. P., "Developing Mechanism-Based Methods for Estimating Hypersonic Boundary-Layer Transition in Flight: The Role of Quiet Tunnels," *Progress in Aerospace Sciences*, Vol. 72, Jan. 2015, pp. 17–29. https://doi.org/10.1016/j.paerosci.2014.09.008

[21] Duan, L., Choudhari, M. M., and Zhang, C., "Pressure Fluctuations Induced by a Hypersonic Turbulent Boundary Layer," *Journal of Fluid Mechanics*, Vol. 804, Oct. 2016, pp. 578–607. https://doi.org/10.1017/jfm.2016.548

[22] Duan, L., Choudhari, M. M., Chou, A., Munoz, F., Radespeil, R., Schilden, T., Schroder, W., Marineau, E., Casper, K., Chaudhry, R., Candler, G., Gray, K., and Schneider, S., "Characterization of Freestream Disturbances in Conventional Hypersonic Wind Tunnels," *Journal of Spacecraft and Rockets*, Vol. 56, No. 2, 2016, pp. 578–607. https://doi.org/10.2514/1.A34290

[23] Marineau, E., Moraru, C., Lewis, D., Norris, J., and Lafferty, J., "Investigation of Mach 10 Boundary Layer Stability of Sharp Cones at Angle-of-Attack, Part 1: Experiments," *53rd AIAA Aerospace Sciences Meeting*, AIAA Paper 2015-1737, 2015. https://doi.org/10.2514/6.2015-1737

[24] Mack, L. M., "Transition and Laminar Instability," NASA Jet Propulsion Lab. CP-153203, Pasadena, CA, 1977.

[25] Paredes, P., Venkatachari, B., Choudhari, M., Li, F., Chang, C., Zafar, M., and Xiao, H., "Effects of Nose Bluntness on Hypersonic Boundary-Layer Receptivity and Stability over Cones," *AIAA Journal*, Vol. 58, No. 10, 2020, pp. 4475–4484. https://doi.org/10.2514/1.J059407

[26] Fedorov, A., and Tumin, A., "The Mack's Amplitude Method Revisited," *Theoretical Computational Fluid Dynamics*, Vol. 36, June 2021, pp. 9–24. https://doi.org/10.1007/s00162-021-00575-x

[27] Marineau, E., "Prediction Methodology for Second-Mode Dominated Boundary-Layer Transition in Wind Tunnels," *AIAA Journal*, Vol. 55, No. 2, 2017, pp. 484–499. https://doi.org/10.2514/1.J055061

[28] Marineau, E., Moraru, C., Lewis, D., Norris, J., and Lafferty, J., "Mach 10 Boundary-Layer Transition Experiments on Sharp and Blunted Cones," *19th AIAA International Space Planes and Hypersonic Systems and Technologies Conference*, AIAA Paper 2014-3108, 2014. https://doi.org/10.2514/6.2014-3108

[29] Johnson, H., Alba, C., Candler, G., Maclean, M., Wadhams, T., and Holden, M., "Boundary-Layer Stability Analysis of the Hypersonic International Flight Research Transition Experiments," *Journal of Spacecraft and Rockets*, Vol. 45, No. 2, 2008, pp. 228–236. https://doi.org/10.2514/1.31878

[30] Alba, C., Johnson, H., Bartkowicz, M., Candler, G., and Berger, K., "Boundary-Layer Stability Calculations for the HIFiRE-1 Transition Experiment," *Journal of Spacecraft and Rockets*, Vol. 45, No. 6, 2008, pp. 1125–1133. https://doi.org/10.2514/1.37445

[31] Huang, Y., "Numerical Study of Hypersonic Boundary-Layer Receptivity and Stability with Freestream Hotspot Perturbations," Ph.D. Thesis, Univ. of California, Los Angeles, 2016.

[32] Kara, K., Balakumar, P., and Kandil, O., "Effects of Nose Bluntness on Hypersonic Boundary-Layer Receptivity and Stability over Cones," *AIAA Journal*, Vol. 49, No. 12, 2011, pp. 2593–2606. https://doi.org/10.2514/1.J050032

[33] He, S., and Zhong, X., "Numerical Study of the Receptivity of a Blunt Cone to Freestream Pulse Disturbances in Hypersonic Flow," *AIAA Aviation 2021 Forum*, AIAA Paper 2021-2887, 2021. https://doi.org/10.2514/6.2021-2887

[34] He, S., "Receptivity of Straight Blunt Cones to Broadband Freestream Pulse Disturbances for Transition Prediction in Hypersonic Flow," Ph.D. Thesis, Univ. of California, Los Angeles, 2022.

[35] Fedorov, A., and Kozlov, M., "Receptivity of High-Speed Boundary Layer to Solid Particulates," *6th AIAA Theoretical Fluid Mechanics Conference*, AIAA Paper 2011-3925, 2011. https://doi.org/10.2514/6.2011-3925

[36] Casper, K., Beresh, S., and Schneider, S., "Comparison of Methods for Determining Boundary Layer Edge Conditions for Transition Correlations," *33rd AIAA Fluid Dynamics Conference and Exhibit*, AIAA Paper 2003-3590, 2003. https://doi.org/10.2514/6.2003-3590

[37] Liechty, D., Berry, S., Hollis, B., and Horvath, T., "Pressure Fluctuations Beneath Turbulent Spots and Instability Wave Packets in a Hypersonic Boundary Layer," *49th AIAA Aerospace Sciences Meeting Including the New Horizons Forum and Aerospace Exposition*, AIAA Paper 2011-0372, 2011. https://doi.org/10.2514/6.2011-372

[38] Paredes, P., Choudhari, M. M., Li, F., Jewell, J. S., Kimmel, R. L., Marineau, E. C., and Grossir, G., "Nose-Tip Bluntness Effects on Transition at Hypersonic Speeds," *Journal of Spacecraft and Rockets*, Vol. 56, No. 2, 2019, pp. 369–387. https://doi.org/10.2514/1.A34277

[39] Stetson, K., "Nosetip Bluntness Effects on Cone Frustum Boundary Layer Transition in Hypersonic Flow," *16th Fluid and Plasmadynamics Conference*, AIAA Paper 1983-1763, 1983. https://doi.org/10.2514/6.1983-1763

[40] Marineau, E., Lewis, D., Michael, S., John, L., White, M., and Amar, A., "Investigation of Hypersonic Laminar Heating Augmentation in the Stagnation Region," *51st AIAA Aerospace Sciences Meeting*, AIAA Paper 2013-0308, 2013. https://doi.org/10.2514/6.2013-0308

[41] Balakumar, P., and Kegerise, M., "Receptivity of Hypersonic Boundary Layers to Acoustic and Vortical Disturbances," *49th AIAA Aerospace Sciences Meeting Including the New Horizons Forum and Aerospace Exposition*, AIAA Paper 2011-0371, 2011. https://doi.org/10.2514/6.2011-371

[42] Egorov, I. V., Fedorov, A. V., Novikov, A. V., and Chuvakhov, P. V., "The Role of Receptivity in Prediction of High-Speed Laminar-Turbulent Transition," *IUTAM Laminar-Turbulent Transition*, edited by S. Sherwin, P. Schmid, and X. Wu, Springer International, Cham, Switzerland, 2022, pp. 541–552. https://doi.org/10.1007/978-3-030-67902-6_47

A. Dufrene
Associate Editor